IEEE Access
Multidisciplinary | Rapid Review | Open Access Journal

Received November 12, 2021, accepted November 22, 2021, date of publication November 25, 2021,
date of current version December 10, 2021.

Digital Object Identifier 10.1109/ACCESS.2021.3130998

Overmodulation Strategy Using DC-Link Shunt Resistor Inverters to Maintain Output Voltage Linearity

SOONHO KWON, DONGKYUN SON, HEESUN LIM, JIHWAN PARK, HYUNJUN BAEK, AND GEUN-HO LEE
Department of Automotive Engineering, Kookmin University, Seoul 02707, South Korea

Corresponding author: Geun-Ho Lee (motor@kookmin.ac.kr)

This work was supported in part by BK21 Program through the National Research Foundation of Korea (NRF) by the Ministry of Education under Grant 5199990814084; and in part by the Technology Innovation Program (or Industrial Strategic Technology Development Program) by the Ministry of Trade, Industry and Energy (MOTIE), South Korea, under Grant 200007447.

ABSTRACT To detect the three-phase current in the complex plane of a DC link shunt inverter, an algorithm for restoring the current is required. In this paper, a method of dividing the detection voltage and the compensation voltage to match the output voltage as much as possible to reduce the total harmonic distortion while restoring the current is proposed. In addition, an overmodulation algorithm for a 12-step output, which corresponds to the largest voltage in a DC link shunt inverter, is proposed, and a current recovery method in the overmodulation region is proposed. To determine how to ensure a linear output voltage, the fundamental frequency of the output voltage is analyzed through a Fourier series, and a new voltage vector whose fundamental frequency amplitude is equal to the amplitude of the command voltage is calculated. Finally, the performance of the proposed algorithm is verified through simulation and experimentation. The output of a motor was increased by using overmodulation, and the harmonics of the current based on the output voltage were analyzed through a Fourier series.

INDEX TERMS Field-oriented control, permanent magnet synchronous motor, three-phase inverter, DC link shunt inverters, total harmonic distortion, linearity, space vector PWM, overmodulation, 12-step, fourier series, modulation index.

I. INTRODUCTION

For field-oriented control (FOC) of BLAC motors such as permanent magnet synchronous motors (PMSMs), it is important to detect the correct current of each phase in a three-phase inverter (TPI) [1], [2]. Current sensors are a popular option for accurate three-phase current detection and are appropriate for high-performance motor control, but they increase the volume and cost of a TPI. Therefore, various methods of detecting the phase current based on the voltage drop of the shunt resistor in a TPI have been studied and adopted [3], [4]. They can be divided into 3-shunt (or 2-shunt) inverters that can directly detect each phase current and DC link shunt inverters (DSIs) that detect each phase current from a DC current according to the pulse width modulation (PWM) output, as shown in Fig. 1. A 3-shunt inverter has the advantage of being able to detect the phase current simply without distortion of the PWM, but it has the disadvantage of requiring at least two shunt resistors [4]–[7]. In addition, each phase current scale and offset may incur error due to the error associated with each shunt resistance, which may lead to current phase unbalance. On the other hand, since a DSI uses one shunt resistor to detect the current of each phase, the configuration cost is low, and phase unbalance caused by resistance errors can be prevented. However, a DSI creates a relatively high amount of total harmonic distortion (THD) because it requires technology to distort the PWM to detect the current. Several studies have developed techniques to detect current using a DSI [8]–[11]. The simplest method to detect current in DSIs is to shift PWM as shown in Fig. 4(b). This method has the advantage that it can be designed simply, but has a relatively high THD due to the imbalance of the zero voltage time and the destruction of the PWM center alignment.

The associate editor coordinating the review of this manuscript and approving it for publication was Kan Liu.

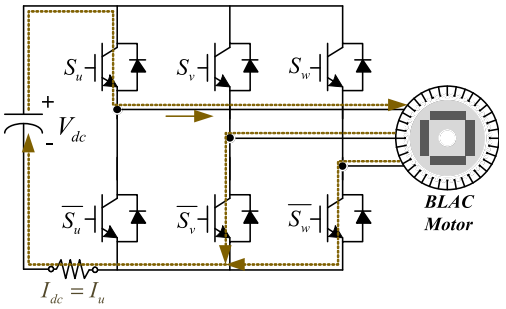

FIGURE 1. Circuit diagram of a DC link shunt inverter.

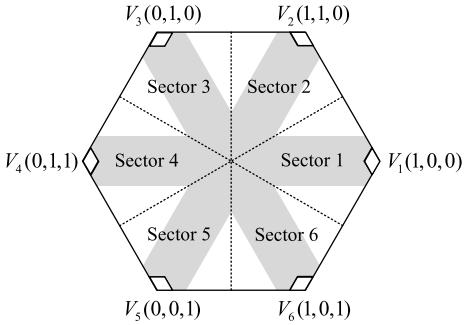

FIGURE 2. Space vector diagram of a DC link shunt inverter.

TABLE 1. DC current value according to the switching state.

Switching State (S_u,S_v,S_w)	DC Current I_{dc} value	Note
(0, 0, 0) (1, 1, 1)	0	Zero voltage
(1, 0, 0)	I_u	V_1
(1, 1, 0)	$-I_w$	V_2
(0, 1, 0)	I_v	V_3
(0, 1, 1)	$-I_u$	V_4
(0, 0, 1)	I_w	V_5
(1, 0, 1)	$-I_v$	V_6

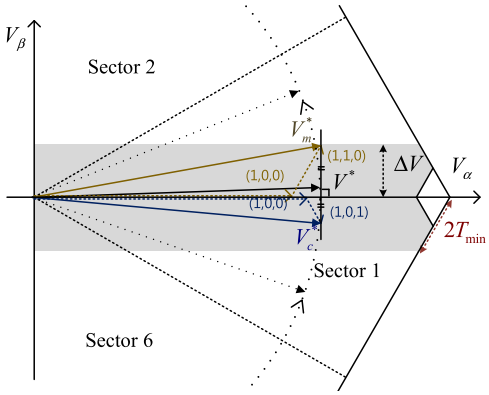

FIGURE 3. Schematic diagram of the current recovery for voltage vectors present in the undetected area (OVIM).

A min-max or space vector PWM (SVPWM) is usually used in a PMSM drive system, but the stator voltage that can be output linearly is limited. To increase the output of a motor or improve the response characteristics, the stator voltage is required rather than the voltage that the TPI can output linearly. Several overmodulation algorithms have been studied and used. Among them, the minimum-phase-error PWM method (MPEPM) and minimum-magnitude-error PWM method (MMEPM) are widely used. Although these algorithms have a relatively simple design, the output voltage in their overmodulation region is nonlinear and cannot be converted linearly with 6-step control, which is required to maximize the output voltage of a TPI [12]–[14]. In the motor control system with a DSI, 6-step control cannot be achieved because of the extent of the area where current cannot be restored, as shown in Fig. 2 (white rhombus area). Instead, 12-step overmodulation which is required to maximize the output voltage in the DSI is used to avoid the area where current cannot be restored.

Several overmodulation algorithms have been proposed in DSI. An overmodulation algorithm using the average voltage vector according to the location of the sampling period is proposed in [15]. An overmodulation method through the combination of a voltage with a phase fixed at the peak of the DSI and a voltage in the linear region is proposed in [16], [17]. An overmodulation method using the superposition principle through the edge voltage of the SVPWM complex plane is proposed in [18], [19]. However, these algorithms require complex calculations to be used on low-performance CPUs.

In this paper, a current recovery algorithm with low THD and a high output voltage utilization rate is proposed for use in a DSI. And, an overmodulation algorithm that can be implemented with relatively simple calculations up to 12-step is proposed. This overmodulation algorithm is a newly proposed method to apply to DSIs, based on the Bolognani overmodulation proposed for general TPIs [20], [21]. In addition, this paper proposes a method of maintaining linearity for the overmodulation output voltage through harmonic analysis using a Fourier series and measures the maximum fundamental voltage according to the proposed algorithm. Finally, the proposed algorithm is verified through a simulation and experiment using SPMSM.

II. CURRENT RECOVERY ALGORITHM

The method of detecting three-phase current in DSI is a method of detecting two-phase current flowing in dc current according to each switching state by applying two effective voltages during one PWM period as shown in Fig. 4. Each effective voltage vector and DC current value according to the switching state are indicated in Table 1. A/D sampling is performed at each effective voltage application time to detect the two-phase current. After detecting the two-phase current, the three-phase current is detected using the theory that the sum of the three-phase currents is zero. However, there is a region where two-phase currents cannot be detected on the complex plane.

Expressing the voltage vector located in the undetectable-current area of Fig. 2 (gray band/Sector 1) as PWM converts

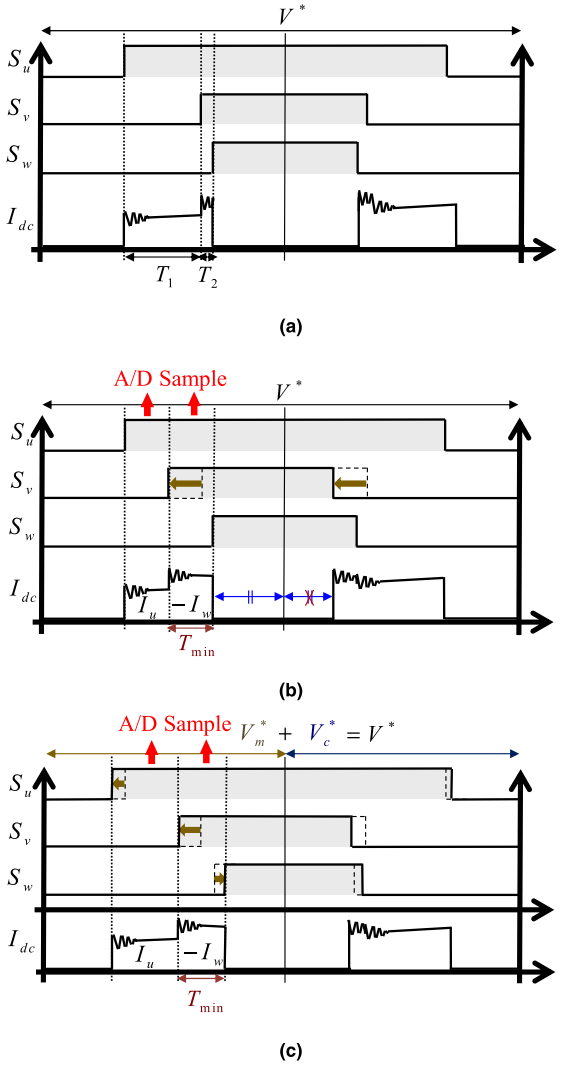

FIGURE 4. Comparison of PWM waveforms: (a) conventional SVPWM waveform, (b) PWM shift method waveform, (c) OVIM PWM waveform.

it into a form similar to that in Fig. 4(a). Since the second effective voltage application time T_2 is less than the minimum time required for current detection $T_{\min}$, only single-phase current can be detected, and accurate current control cannot be achieved. Therefore, to detect two-phase current, the output PWM in the undetected area must be distorted. $T_{\min}$ is defined as follows [4]–[6].

$$T_{\min} = T_{dead} + T_{sat} + T_{A/D} \tag{1}$$

where T_{dead} is the dead time required to prevent an arm short circuit; T_{sat} is the saturation time required for the voltage to reach steady state; and $T_{A/D}$ is the analog-to-digital conversion time of the digital signal processor (DSP).

The method proposed in this paper for recovering the current in the undetected area, called the optimal voltage injection method (OVIM), is shown in Fig. 3. The OVIM measures the current by dividing the command voltage in the undetected area into a current measurement voltage vector and a compensation vector and applying each over a half-cycle. To lower the THD of the output voltage, the two voltages are divided orthogonally to the α-axis to minimize the two voltage intervals.

$$\begin{aligned} V^* &= \left|V^*\right| e^{j\theta^*} \\ V^* T_s &= (V_m^* + V_c^*) \times 0.5 T_s \end{aligned} \tag{2}$$

where T_s is the current sampling period for motor control; V^* is the command voltage vector; θ^* is the phase of the command voltage; V_m^* is the voltage vector for current measurement; and V_c^* is the compensation voltage vector.

A new coordinate transformation is required to convert the voltage vector of each sector to the α-β axis of sector 1 to determine whether the voltage vector is present in the undetected area. The coordinate transformation equation is as follows.

$$\begin{aligned} \theta &= \theta^* - (n-1)\frac{\pi}{3} \quad (n = 1, 2, 3, 4, 5, 6) \\ V_\alpha^* &= \left|V^*\right| \cos\theta, \quad V_\beta^* = \left|V^*\right| \sin\theta \end{aligned} \tag{3}$$

where V_α^* and V_β^* are the α-β axis voltages.

Comparing the magnitude of the β-axis command voltage and ΔV in Fig. 3 reveals whether the command voltage is present in the undetected area. If $\left|V_\beta^*\right| < \Delta V$, then the command voltage vector is present in the undetected area, and the OVIM for current detection should be applied. ΔV, V_m, and V_c can be calculated as follows.

$$\Delta V = \frac{2T_{\min}}{\sqrt{3}T_s} V_{dc} \tag{4}$$

$$V_m^* = \begin{cases} V_\alpha^* + j(V_\beta^* + \Delta V - V_\beta^*) & (V_\beta^* \geq 0) \\ V_\alpha^* + j(V_\beta^* - \Delta V - V_\beta^*) & (V_\beta^* < 0) \end{cases} \tag{5}$$

$$V_c^* = \begin{cases} V_\alpha^* + j(V_\beta^* - \Delta V + V_\beta^*) & (V_\beta^* \geq 0) \\ V_\alpha^* + j(V_\beta^* + \Delta V + V_\beta^*) & (V_\beta^* < 0) \end{cases} \tag{6}$$

The OVIM is compared to conventional PWM in Fig. 4. The conventional SVPWM and DC current waveforms of the voltage in the undetectable-current area are shown in Fig. 4(a), and the PWM and DC current waveforms to which OVIM is applied are shown in Fig. 4(c). The U-phase and W-phase currents are detected by applying the measured voltage during the PWM half-cycle, and the compensation voltage is applied during the next half-cycle to restore the two sum vectors to the original command voltage vector.

As shown in Fig. 5(a), In the area of triangles ABC and CDE at the vertices of a complex vector, V_m^* and V_c^* cannot exist orthogonal to the a-axis. To detect three-phase current, the measured voltage V_m^* must be output outside the gray band area. Therefore, the current can be restored by moving V_c^* to maintain the magnitude and phase of the command voltage vector V^*. To identify this area, the maximum OVIM output voltage $V_{OVIM\,\max}$ is calculated as follows.

$$V_{OVIM\,\max} = \frac{2}{3} V_{dc} \left(1 - \frac{T_{\min}}{T_s}\right) \tag{7}$$

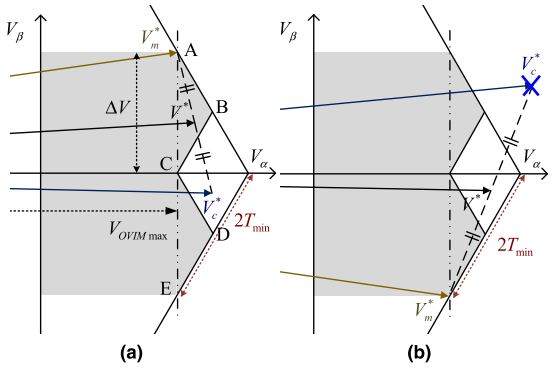

FIGURE 5. Schematic diagram of the OVIM: (a) when measurement voltage vector and compensation voltage vector do not exist orthogonally, (b) when the voltage vector exists in the region where the current cannot be restored.

V_m^* and V_c^* can be recalculated as follows.

$$V_m^* = \begin{cases} V_\alpha^* - V_\alpha^* + V_{OVIM\max} + j(V_\beta^* + \Delta V - V_\beta^*) \\ \qquad (V_\beta^* \geq 0) \\ V_\alpha^* - V_\alpha^* + V_{OVIM\max} + j(V_\beta^* - \Delta V - V_\beta^*) \\ \qquad (V_\beta^* < 0) \end{cases} \tag{8}$$

$$V_c^* = \begin{cases} V_\alpha^* + V_\alpha^* - V_{OVIM\max} + j(V_\beta^* - \Delta V + V_\beta^*) \\ \qquad (V_\beta^* \geq 0) \\ V_\alpha^* + V_\alpha^* - V_{OVIM\max} + j(V_\beta^* + \Delta V + V_\beta^*) \\ \qquad (V_\beta^* < 0) \end{cases} \tag{9}$$

As shown in Fig. 5(b), when the output voltage is divided by the measured voltage V_m^* and the compensation voltage V_c^* in the corner region (white rhombus) of the complex plane, it cannot be output because V_c^* is out of the complex plane. Therefore, the voltage vector in the white rhombus of the SVPWM complex plane cannot be output because it is physically impossible to restore the current.

III. OVERMODULATION

The overmodulation algorithm proposed in this section is a maintain-voltage-magnitude overmodulation (MVMO) algorithm capable of a maximum 12-step operation, which is achieved by maintaining the magnitude of the command voltage in the DSI.

The MVMO algorithm uses a circle with a radius that is the size of the command voltage in the overmodulation region and is larger than the inscribed circle of the SVPWM complex plane. When the position of the voltage vector is within the SVPWM complex plane, the normal SVPWM method is used. When the position of the voltage vector is outside, the phase is fixed to the closest intersection with the voltage vector among the intersections of the circle with a radius the size of the command voltage, the area of which is where current recovery is possible. When applying the MVMO algorithm, the output phase is divided in two according to the size of the command voltage vector.

A. BOLOGNANI OVERMODULATION DRIVE

In this case, the circle of the command voltage does not contain the white rhombus area in Fig. 2 and can be defined by the following equation.

$$\frac{V_{dc}}{\sqrt{3}} < \left|V^*\right| < V_{OVIM\max} \tag{10}$$

If the voltage vector is outside the SVPWM complex plane, the phase is fixed at the hold angle α to maintain the magnitude of the output voltage. The hold angle, which is based on the magnitude of the voltage vector, can be obtained using a trigonometric function.

$$\alpha = \frac{\pi}{6} - \arccos\frac{\sqrt{3} \times |V^*|}{V_{dc}} \tag{11}$$

Then, the phase of the output voltage $V^{*\prime}$, which is based on the command voltage phase ($0 \leq \theta < \pi/3$), is defined as follows (Figs. 6(a) and (d)).

$$\theta_{ovm} = \begin{cases} \theta & (0 \leq \theta < \alpha) \\ \alpha & (\alpha \leq \theta < \pi/6) \\ \pi/3 - \alpha & (\pi/6 \leq \theta < \pi/3 - \alpha) \\ \theta & (\pi/3 - \alpha \leq \theta < \pi/3) \end{cases} \tag{12}$$

The hold angle changes with the magnitude of the command voltage vector and approaches 0 degrees as the magnitude of the voltage increases. However, if the amplitude of the voltage vector in the DSI is greater than $V_{OVIM\max}$, another phase angle must be considered.

B. 12-STEP OVERMODULATION DRIVE

In this case, the circle denoting the command voltage contains the white rhombus area in Fig. 2 and can be defined by the following equation.

$$V_{OVIM\max} \leq \left|V^*\right| \leq V_{ref\max} \tag{13}$$

The phase is fixed not only at the hold angle but also at the intersection of the reference voltage circle and the white rhombus. $V_{ref\max}$ is the maximum output voltage (12-step) usable in the proposed overmodulation algorithm and can be calculated as follows.

$$V_{ref\max} = \frac{2}{3}V_{dc}\left(1 - \frac{T_{\min}}{2T_s}\right) \tag{14}$$

Then, the phase of the output voltage $V^{*\prime}$, which is based on the command voltage phase ($0 \leq \theta < \pi/3$), is as follows (Figs. 6(b) and (e)).

$$\theta_{ovm} = \begin{cases} \alpha_{rh} & (0 \leq \theta < \alpha_{rh}) \\ \theta & (\alpha_{rh} \leq \theta < \alpha) \\ \alpha & (\alpha \leq \theta < \pi/6) \\ \pi/3 - \alpha & (\pi/6 \leq \theta < \pi/3 - \alpha) \\ \theta & (\pi/3 - \alpha \leq \theta < \pi/3 - \alpha_{rh}) \\ \pi/3 - \alpha_{rh} & (\pi/3 - \alpha_{rh} \leq \theta < \pi/3) \end{cases} \tag{15}$$

α_{rh} is the phase angle for delaying the voltage phase in the area where current recovery is impossible in the DSI and

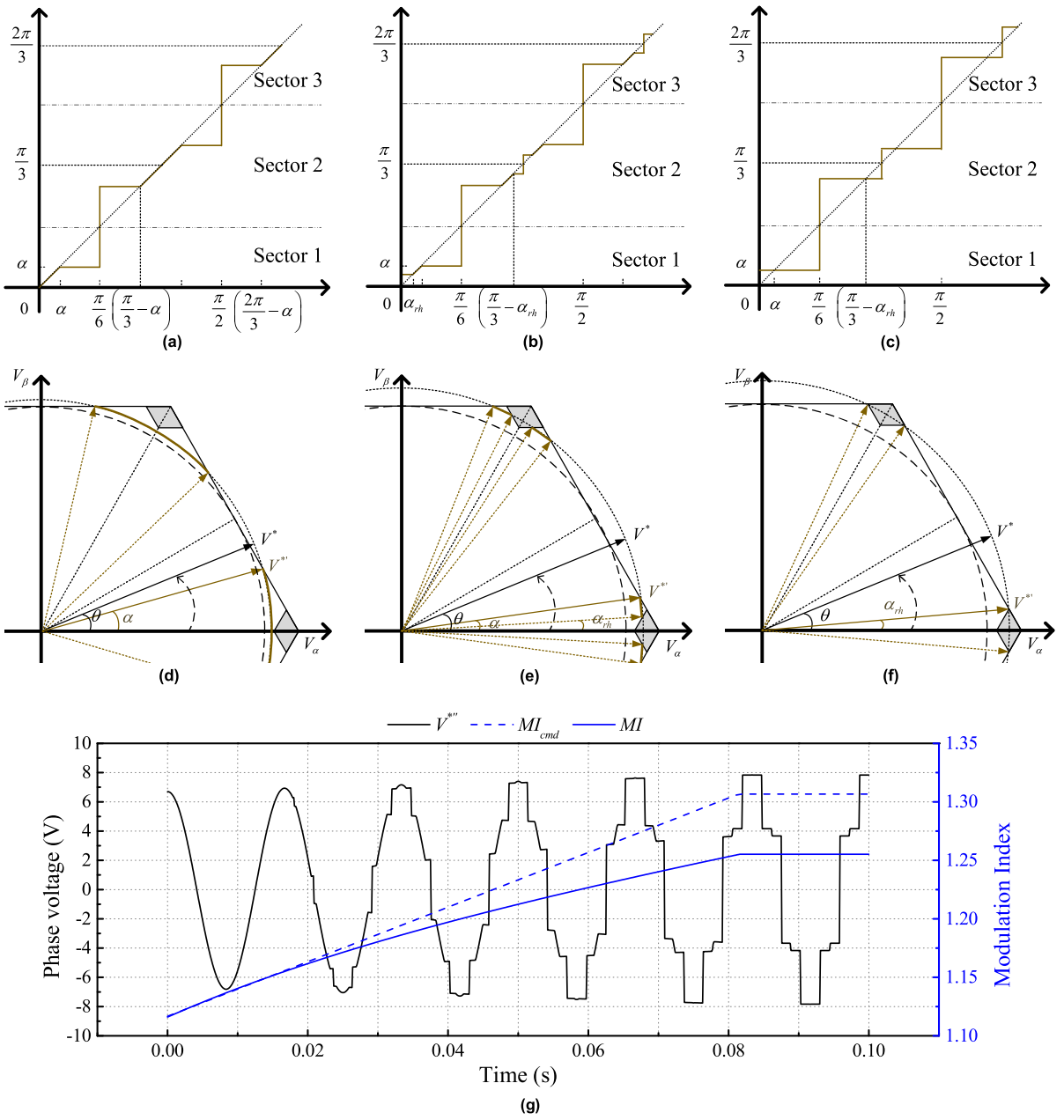

FIGURE 6. Schematic diagram of the MVMO: (a) phase of the output voltage under Bolognani overmodulation drive, (b) phase of the output voltage under MVMO drive, (c) phase of the output voltage under 12-step drive, (d) space vector diagram under Bolognani overmodulation drive, (e) space vector diagram under MVMO drive, (f) space vector diagram under 12-step drive, (g) phase voltage wave form and comparison of modulation index.

is shown in Fig. 7. To output the command voltage V^*, the voltage vector $V^{*\prime}$ must be output with the same amplitude and a vector direction toward the hypotenuse of the rhombus. However, it is difficult to calculate the phase angle of the voltage vector $V^{*\prime}$, which requires a complicated calculation based on $T_{\min}$. Therefore, the output voltage is replaced with a new proximity voltage vector $V^{*\prime\prime}$, which has a phase and magnitude close to those of $V^{*\prime}$ and is easy to calculate. Increasing $T_{\min}$ increases the error associated with the two voltage vectors, but when $T_{\min}$ is small, the error is negligible ($V^{*\prime} \approx V^{*\prime\prime}$). Even if the error is large, it can be neglected because the voltage is output through fundamental harmonic analysis via the Fourier series. V_{offset} is the size to be added to the β-axis command voltage to obtain $V^{*\prime\prime}$ and is calculated as follows.

$$V_{\Delta\alpha} = V_{ref\,\max} - V_\alpha^*, \quad V_{\Delta\beta} = \sqrt{3} \times V_{\Delta\alpha} \tag{16}$$

$$V_{offset} = V_{\Delta\beta} - V_\beta^* \tag{17}$$

The new voltage vector ($V^{*\prime\prime}$) is calculated as follows.

$$V^{*\prime\prime} = V_\alpha^{*\prime\prime} + jV_\beta^{*\prime\prime}$$
$$V_\alpha^{*\prime\prime} = V_\alpha^*, \quad V_\beta^{*\prime\prime} = V_\beta^* + V_{offset} \tag{18}$$

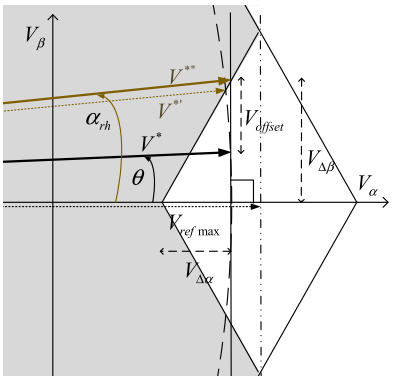

FIGURE 7. Schematic diagram of the MVMO when voltage vector is in a region where current cannot be restored.

$$\alpha_{rh} = \tan^{-1}\left(\frac{V_\beta^{*\prime\prime}}{V_\alpha^{*\prime\prime}}\right) \tag{19}$$

In the proposed MVMO algorithm, as the command voltage increases, the hold angle α decreases, and the rhombus angle α_{rh} increases. As the two phases become increasingly similar, a smooth conversion is performed linearly with 12-step control, as shown in Figs. 6(c) and (f).

IV. ANALYSIS OF VOLTAGE HARMONICS

The phase voltage output by the MVMO algorithm, as shown in Fig. 6(g), changes from a sine wave to a square wave and contains many harmonics. Except for the fundamental component used for actual control, the harmonics are lossy components such as noise and ripple. Since the size of the fundamental frequency used for actual control is smaller than the size of the output voltage, the voltage is nonlinear. Prior to the description, the voltage modulation index (*MI*) indicating the magnitude of the fundamental frequency included in the output phase voltage is defined as follows.

$$MI = \frac{|V_{1st}|}{0.5V_{dc}} \tag{20}$$

To compare the fundamental wave to the output voltage, the voltage *MI* of the command voltage is defined as follows.

$$MI_{cmd} = \frac{|V^*|}{0.5V_{dc}} \tag{21}$$

In this section, harmonic analysis of the output voltage is performed through the Fourier series during MVMO operation. In addition, an improved method for maintaining the linearity of the output voltage is proposed.

The Fourier series of a general function with a specific period is as follows.

$$\begin{aligned} f(t) &= a_0 + \sum_{n=1}^{\infty} c_n \sin(n\omega t + \phi_n) \\ &= a_0 + \sum_{n=1}^{\infty} (a_n \cos n\omega t + b_n \sin n\omega t) \end{aligned} \tag{22}$$

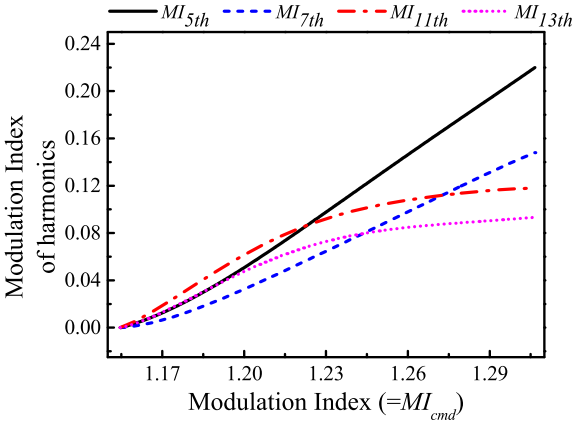

FIGURE 8. Modulation index of harmonics analysis with MVMO.

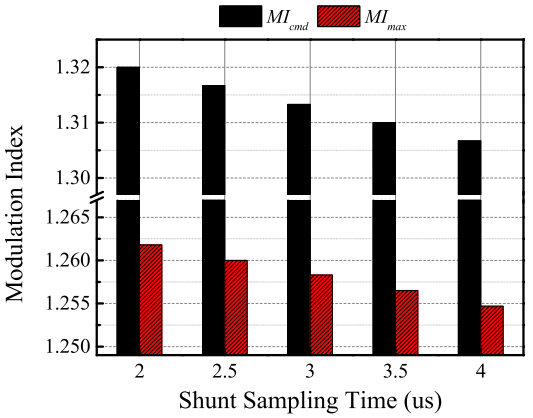

FIGURE 9. Fundamental frequency modulation index according to shunt sampling time.

$$\begin{aligned} a_0 &= \frac{1}{T}\int_0^T f(t)dt, \quad c_n = \sqrt{a_n^2 + b_n^2}, \ \phi_n = \tan^{-1}\left(\frac{a_n}{b_n}\right) \\ a_n &= \frac{2}{T}\int_0^T f(t)\cos n\omega t dt, \quad b_n = \frac{2}{T}\int_0^T f(t)\sin n\omega t dt \end{aligned} \tag{23}$$

Since the voltages of the output 3 phase are even functions ($f(x) = f(-x)$) and have a phase difference of 120 degrees, the Fourier series for the phase voltage can be reorganized as follows.

$$a_0 = 0, \ a_{2n} = 0, \ a_{3n} = 0, \ b_n = 0 \tag{24}$$

$$\begin{aligned} V(t) = {} & V_{1st}\cos\omega t + V_{5th}\cos 5\omega t + V_{7th}\cos 7\omega t \\ & + V_{11th}\cos 11\omega t + V_{13th}\cos 13\omega t + \cdots \end{aligned} \tag{25}$$

The phase voltage output from overmodulation is composed of the fundamental frequency and the 5th, 7th, 11th, and 13th harmonics, as shown in Fig. 8. The magnitude of the command voltage and the magnitude of the phase voltage used for motor control have an error in the sum of harmonics, resulting in a nonlinear characteristic. The nonlinearity of

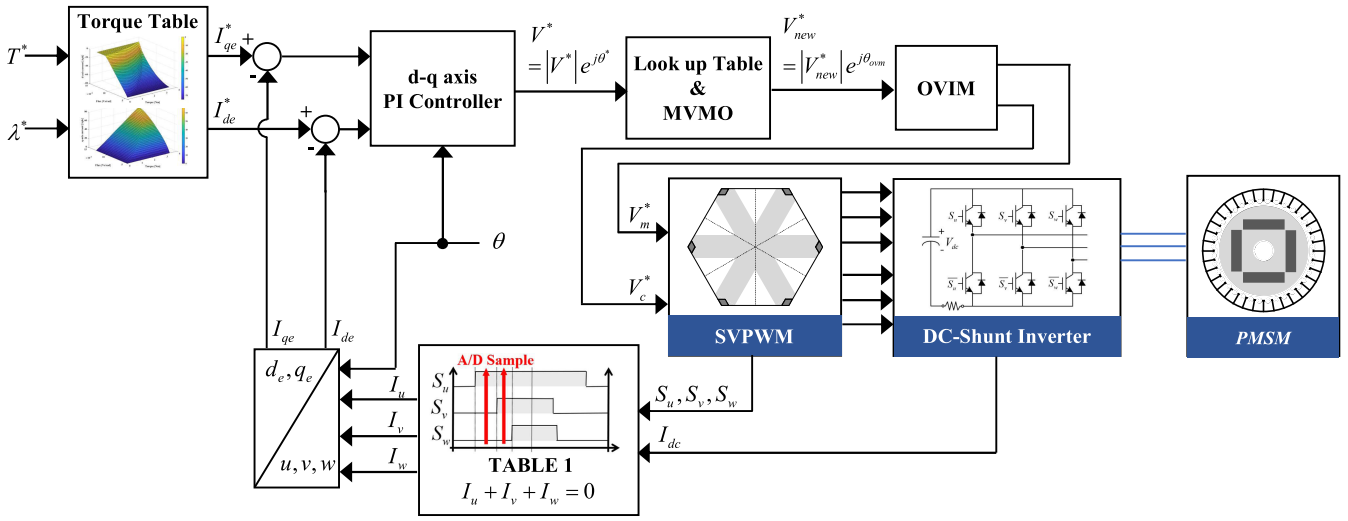

FIGURE 10. Block diagram of PMSM vector control used in simulation and experiment to verify the proposed algorithm.

the output voltage causes the current controller to have low dynamic characteristic. To maintain linearity, the *MI* of the fundamental frequency according to the output phase voltage is analyzed off-line through the Fourier series, as shown in Fig. 6(g), and a look-up table is applied. Linearity is maintained by using a phase voltage whose fundamental frequency has the same magnitude as the output voltage of the current controller. Fig. 11 is a block diagram of MVMO overmodulation using the voltage *MI*.

$$V^*_{new} = LT\left(\left|V^*\right|\right), \quad V_1 = \left|V^*\right|$$
$$V^*_{new}(t) = V_1 \cos\omega t + V_5 \cos 5\omega t + V_7 \cos 7\omega t + \cdots \tag{26}$$
$$MI_{\max} = \frac{LT^{-1}\left(\left|V_{ref\,\max}\right|\right)}{0.5V_{dc}} \tag{27}$$

$MI_{\max}$ is the maximum voltage *MI* of the fundamental frequency that can be output according to $T_{\min}$. As the output phase voltage of the proposed MVMO method decreases in proportion to $T_{\min}$, as shown in Equation (14) and (27), the magnitude of the fundamental frequency also decreases. Fig. 9 shows an off-line analysis of the maximum output phase voltage and the maximum voltage *MI* of the fundamental frequency *MI* according to $T_{\min}$.

V. SIMULATION AND EXPERIMENT

To verify the algorithm proposed in this paper, simulation using MATLAB, and experiments were performed using motors and inverters with the specifications shown in Table 2. The PMSM control block diagram used in the simulation and experiment was composed of a DC link shunt 2-level voltage source inverter, as shown in Fig. 10. The field attenuation technique for high-speed operation was implemented using a magnetic flux-torque table; refer to reference [22], [23] for a detailed algorithm.

TABLE 2. Motor and inverter specifications.

Description	Value
Motor type	SPMSM
Pole	4
DC-Voltage [V]	12
Rated Current [A]	15
Max. operation speed [rpm]	9900
Max. torque [Nm]	0.182
DC link Shunt Resistor [mΩ]	2
T_{min} [usec]	3
Switch frequency [kHz]	10

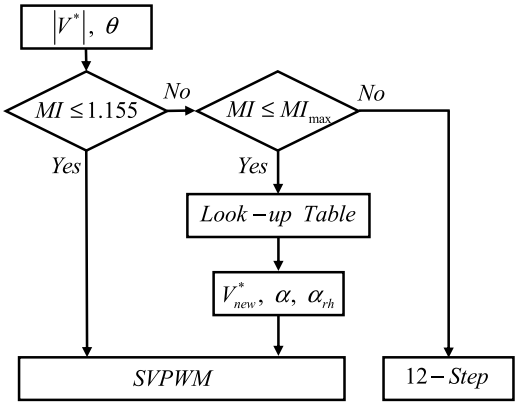

FIGURE 11. Block diagram of the MVMO based on look-up table.

A. SIMULATION

The maximum voltage ($V_{ref\,\max}$) that can be output in this experiment and the maximum modulation index ($MI_{\max}$) of the fundamental frequency are as follows.

$$V_{ref\,\max} = \frac{2}{3}V_{dc}\left(1 - \frac{T_{\min}}{2T_s}\right) = 7.88[V], \quad MI_{\max} \approx 1.258 \tag{28}$$

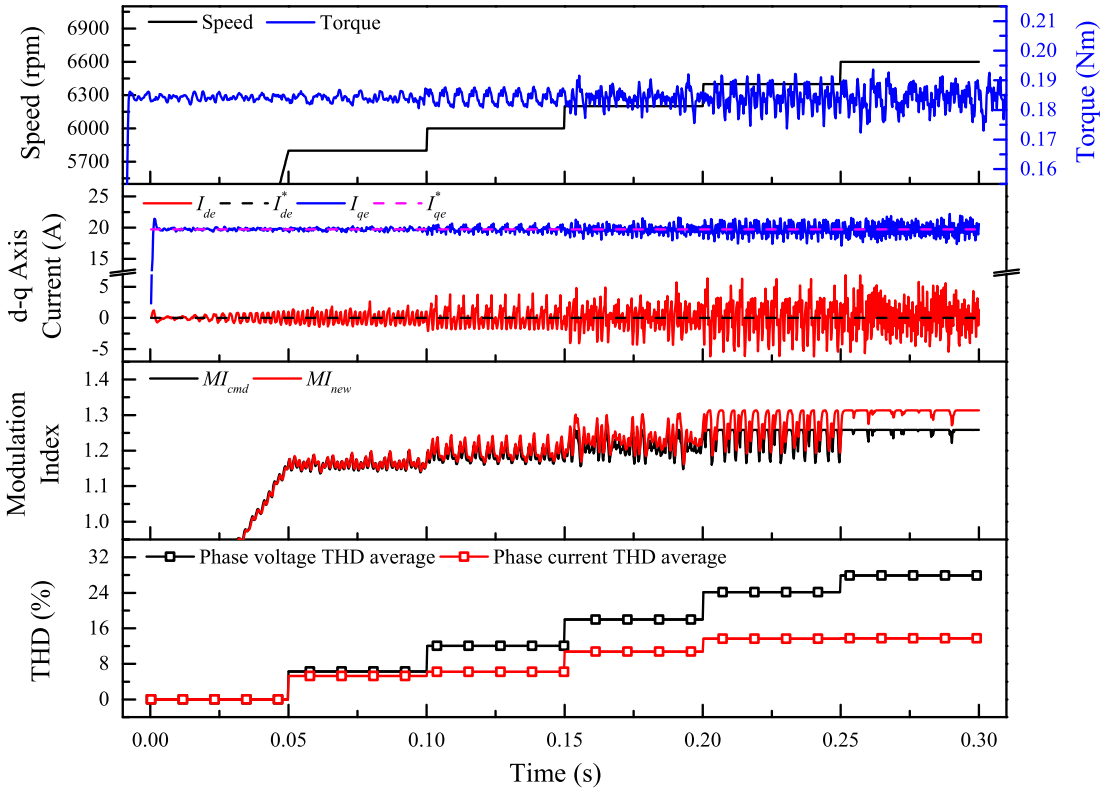

FIGURE 12. Block diagram of PMSM vector control used in simulation and experiment to verify the proposed algorithm.

$MI_{\max}$ was measured by off-line fast Fourier transform (FFT) analysis of the simulation results for use in actual experiments. Through FFT analysis of the simulation results, the amplitude of the fundamental frequency was analyzed for each *MI* size, as shown in Fig. 6(g), and MVMO was applied to the experiment. Fig. 13 shows the α-β axis voltage data obtained by measuring the output voltage vector for each control period while increasing the *MI* from 1.175 to 1.258 at a constant rate through simulation. As the *MI* increases, the output voltage vector approaches the 12-step value along the hypotenuse of the SVPWM complex plane. Fig. 14 depicts a waveform comparing the voltage *MI* of the fundamental wave voltage according to the command voltage *MI* for MVMO, MMEPM and MPEPM, respectively. MMEPM and MPEPM cannot output up to the maximum voltage that can be output from a DSI, but MVMO can output up to $MI_{\max}$. Additionally, when a look-up table is used, the output voltage is linear, like a unit vector. Fig. 12 shows the simulation results of d-q axis current, torque, *MI*, and THD according to speed. It was confirmed that the MVMO output MI_{cmd} increased linearly to $MI_{\max}$ (12-step driving) as the speed increased. MI_{new} is the voltage command applied to the motor as the output value of the lookup table through the MVMO algorithm. As the phase voltage approaches 12-step operation, the THD of the phase voltage and the phase current also increase, so it was confirmed that harmonics are included in the d-q axis current and torque feedback. But the average

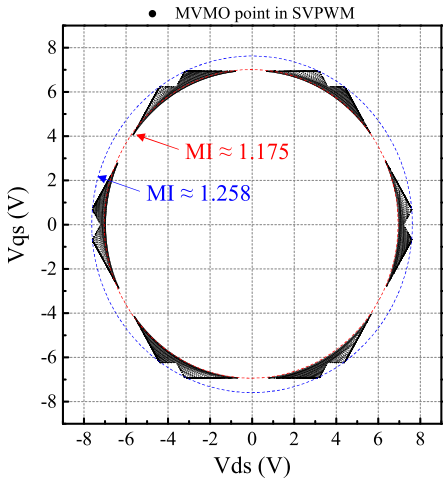

FIGURE 13. Simulation result: MVMO output point in α-β axis.

of the torque was maintained. It was confirmed that as the THD of the voltage increased, the THD of the current also increased. But, even if the same phase voltage is input to the motor, only the THD trend of the current according to the THD of the voltage can be confirmed in this experiment because the THD of the current is greatly affected by various variables such as the motor parameter, the cut-off frequency of the current controller, and the switching frequency.

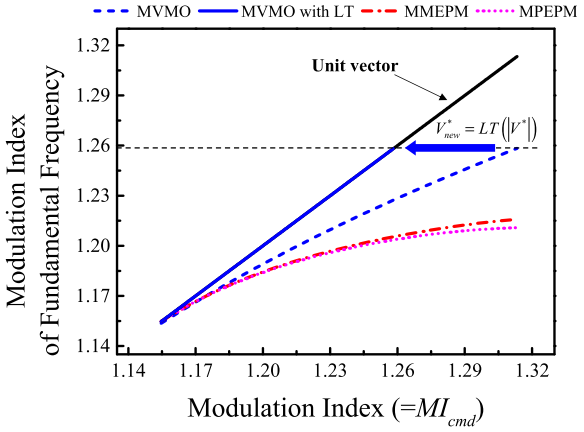

FIGURE 14. Linearity comparison of overmodulation algorithms.

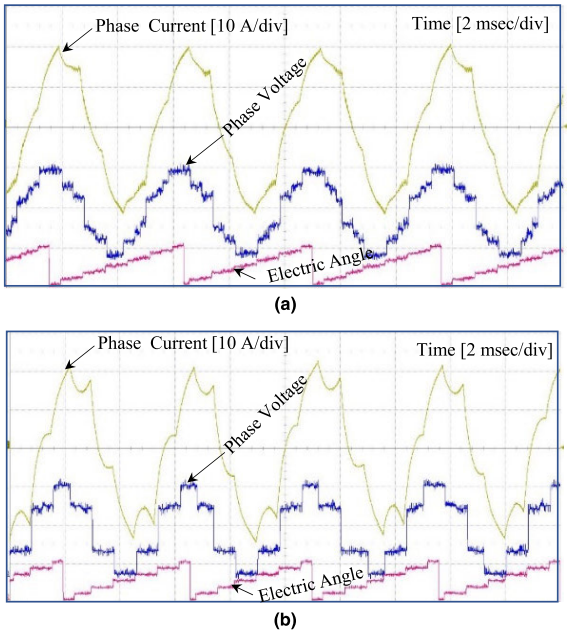

FIGURE 15. Experimental results of phase current, phase voltage, and phase angle waveform: (a) $1.155 < MI < MI_{max}$, (b) $MI = MI_{max}$.

B. EXPERIMENTAL RESULTS

Fig. 15 shows the results of voltage and current experiments applying the proposed algorithm to a DSI. Fig. 15(a) presents the result of MVMO control in $1.155 \leq MI < MI_{\max}$; the operating conditions consisted of a 0.18 Nm output at 6250 rpm. Based on the phase and phase voltage of the output voltage vector, the operation of the proposed MVMO can be confirmed. Fig. 15(b) is the result of MVMO control at $MI = MI_{\max}(= 1.258)$. The 12-step voltage is output under operating conditions consisting of 0.18 Nm output at 6800 rpm. The 12-step voltage includes the 5th, 7th, 11th, and 13th harmonics, so the current also becomes a waveform including harmonics rather than sinusoids. Fig. 16 shows an FFT analysis of the phase current waveform in the operating state of Fig. 15(a). Current was measured according to the conventional SVPWM method, the proposed OVIM method, and the PWM shift method, and THD was analyzed to be 11.61%, 12.24%, and 13.86%, respectively. In inverters using current sensors, the conventional SVPWM method has the lowest THD because no PWM distortion is required to detect the current. The PWM shift method was analyzed with a relatively high THD, and the OVIM was analyzed with a THD value close to that of the conventional SVPWM method in an inverter using current sensors. Fig. 17 shows the T-N curve and output measurement data before and after the application of the proposed overmodulation algorithm. Before the MVMO was applied, the voltage *MI* was 1.098 (= 1.155 * 0.95) including 5% margin in SVPWM linear output to prevent control diffusion due to saturation of the current controller (PI controller). After the MVMO was applied, the voltage *MI* increased 1.1457 times to 1.258, and the output increased accordingly.

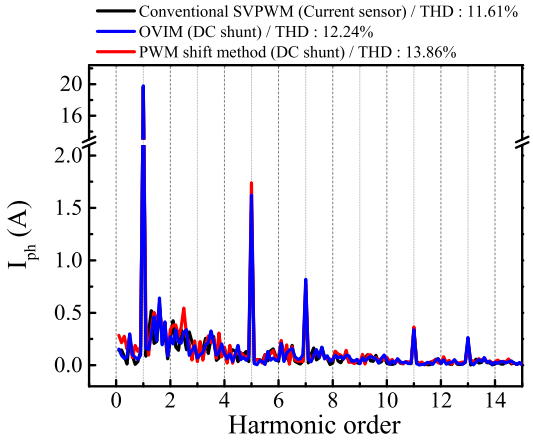

FIGURE 16. Harmonic analysis of current in overmodulation drive.

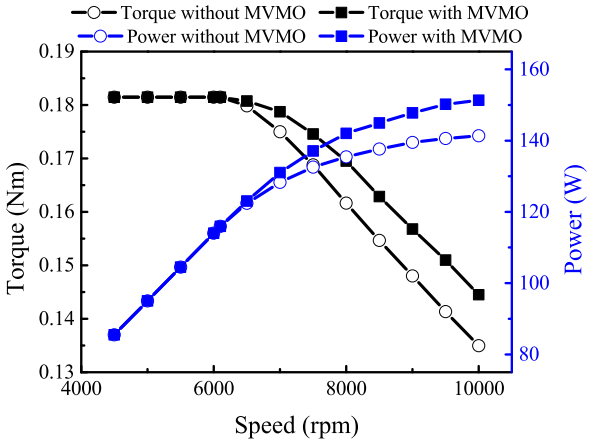

FIGURE 17. Torque and power comparison among the MVMO drive and conventional SVPWM drive(without MVMO).

VI. CONCLUSION

In this paper, an overmodulation algorithm is proposed in DSI with current undetectable area. For 12-step operation in the current undetectable area, an approximate

voltage was calculated, and the voltage amplitude was maintained by fixing the phase with the hold angle. Frequency analysis was performed for the output voltage through a Fourier series, and a look-up table based on the amplitude of the fundamental frequency was designed to maintain linearity. The proposed algorithm is guaranteed to maintain voltage linearity with a relatively simple equation in DSI. It is believed to be an effective and logical overmodulation method in DSI by providing a transition while maintaining linearity to 12-step. The simulation and experimental results provided the feasibility of the proposed method.

REFERENCES

[1] D.-W. Chung and S.-K. Sul, "Analysis and compensation of current measurement error in vector-controlled AC motor drives," *IEEE Trans. Ind. Appl.*, vol. 34, no. 2, pp. 340–345, Mar. 1998, doi: 10.1109/28.663477.

[2] H.-S. Jung, J.-M. Kim, C.-U. Kim, and C. Choi, "Diminution of current measurement error for vector controlled AC motor drives," in *Proc. IEEE Int. Conf. Electr. Mach. Drives*, May 2005, pp. 551–557, doi: 10.1109/IEMDC.2005.195777.

[3] S. Chi, X. Wang, Y. Yuan, Z. Zhang, and L. Xu, "A current reconstruction scheme for low-cost PMSM drives using shunt resistors," in *Proc. 22nd Annu. IEEE Appl. Power Electron. Conf. Expo. (APEC)*, Feb. 2007, pp. 1701–1706, doi: 10.1109/APEX.2007.357748.

[4] D.-Y. Kim, J.-H. Lee, T.-K. Lee, and C.-Y. Won, "Phase current sensing method using three shunt resistor for AC motor drive," in *Proc. IEEE Vehicle Power Propuls. Conf.*, Oct. 2012, pp. 78–82, doi: 10.1109/VPPC.2012.6422566.

[5] B.-G. Cho, J.-I. Ha, and S.-K. Sul, "Analysis of the phase current measurement boundary of three shunt sensing PWM inverters and an expansion method," *J. Power Electron.*, vol. 13, no. 2, pp. 232–242, Mar. 2013, doi: 10.6113/JPE.2013.13.2.232.

[6] Y.-H. Jang, D.-Y. Kim, A.-Y. Ko, I.-K. Won, Y.-R. Kim, and C.-Y. Won, "Three phase current reconstruction method using predictive current in three shunt sensing PWM inverter," in *Proc. IEEE Transp. Electrific. Conf. Expo, Asia–Pacific (ITEC Asia–Pacific)*, Jun. 2016, pp. 436–440, doi: 10.1109/ITEC-AP.2016.7512993.

[7] B.-G. Cho, J.-I. Ha, and S.-K. Sul, "Voltage injection method for boundary expansion of output voltages in three shunt sensing PWM inverters," in *Proc. 8th Int. Conf. Power Electron. (ECCE Asia)*, May 2011, pp. 411–415, doi: 10.1109/ICPE.2011.5944564.

[8] J.-L. Ha, "Voltage injection method for three-phase current reconstruction in PWM inverters using a single sensor," *IEEE Trans. Power Electron.*, vol. 24, no. 3, pp. 767–775, Mar. 2009, doi: 10.1109/TPEL.2008.2009451.

[9] W.-C. Lee, D.-S. Hyun, and T.-K. Lee, "A novel control method for three-phase PWM rectifiers using a single current sensor," *IEEE Trans. Power Electron.*, vol. 15, no. 5, pp. 861–870, Sep. 2000, doi: 10.1109/63.867675.

[10] H.-B. Yeom, H.-K. Ku, and J.-M. Kim, "Current reconstruction method for PMSM drive system with a DC link shunt resistor," in *Proc. IEEE Energy Convers. Congr. Expo. (ECCE)*, Sep. 2016, pp. 1–6, doi: 10.1109/ECCE.2016.7854980.

[11] G. Wang, F. Chen, N. Zhao, Y. Bai, B. Li, S. Liu, and D. Xu, "Current reconstruction considering time-sharing sampling errors for single DC-link shunt motor drives," *IEEE Trans. Power Electron.*, vol. 36, no. 5, pp. 5760–5770, May 2021, doi: 10.1109/tpel.2020.3029335.

[12] D.-C. Lee and G.-M. Lee, "A novel overmodulation technique for space-vector PWM inverters," *IEEE Trans. Power Electron.*, vol. 13, no. 6, pp. 1144–1151, Nov. 1998, doi: 10.1109/63.728341.

[13] T. H. Nguyen, T. L. Van, D.-C. Lee, J.-H. Park, and J.-H. Hwang, "Control mode switching of induction machine drives between vector control and V/f control in overmodulation range," *J. Power Electron.*, vol. 11, no. 6, pp. 846–855, Nov. 2011, doi: 10.6113/JPE.2011.11.6.846.

[14] Y.-C. Kwon, S. Kim, and S.-K. Sul, "Six-step operation of PMSM with instantaneous current control," *IEEE Trans. Ind. Appl.*, vol. 50, no. 4, pp. 2614–2625, Jul./Aug. 2014, doi: 10.1109/TIA.2013.2296652.

[15] J. Park, S. Jung, and J.-I. Ha, "Phase current reconstruction with single DC-link current sensor for six-step operation in three phase inverter," in *Proc. IEEE Energy Convers. Congr. Expo. (ECCE)*, Sep. 2015, pp. 906–912, doi: 10.1109/ECCE.2015.7309784.

[16] H. Lee, S. Hong, J. Choi, K. Nam, and J. Kim, "Sector-based analytic overmodulation method," *IEEE Trans. Ind. Electron.*, vol. 66, no. 10, pp. 7624–7632, Oct. 2019, doi: 10.1109/TIE.2018.2883270.

[17] B. Jung, T. Lee, and K. Nam, "Overmodulation strategy for inverters with a single DC-link current sensor," in *Proc. IEEE Energy Convers. Congr. Expo. (ECCE)*, Oct. 2020, pp. 2649–2655, doi: 10.1109/ECCE44975.2020.9235740.

[18] J.-S. Lee, W.-S. Im, and J.-M. Kim, "An overmodulation method for space vector PWM inverters with DC-link shunt resistor," in *Proc. 8th Int. Conf. Power Electron. (ECCE Asia)*, May 2011, pp. 1997–2004, doi: 10.1109/ICPE.2011.5944465.

[19] K. Sun, Q. Wei, L. Huang, and K. Matsuse, "An overmodulation method for PWM-inverter-fed IPMSM drive with single current sensor," *IEEE Trans. Ind. Electron.*, vol. 57, no. 10, pp. 3395–3404, Oct. 2010, doi: 10.1109/TIE.2009.2038336.

[20] S. Bolognani and M. Zigliotto, "Novel digital continuous control of SVM inverters in the overmodulation range," *IEEE Trans. Ind. Appl.*, vol. 33, no. 2, pp. 525–530, Mar. 1997, doi: 10.1109/28.568019.

[21] S. Bolognani and M. Zigliotto, "Space vector Fourier analysis of SVM inverters in the overmodulation range," in *Proc. Int. Conf. Power Electron., Drives Energy Syst. Ind. Growth*, 1996, pp. 319–324, doi: 10.1109/PEDES.1996.539559.

[22] C. Bianchini, G. Franceschini, and A. Torreggiani, "Improvement on flux weakening control strategy for electric vehicle applications," *Appl. Sci.*, vol. 11, no. 5, p. 2422, Mar. 2021, doi: 10.3390/app11052422.

[23] B. H. Bae, N. Patel, S. Schulz, and S. K. Sul, "New field weakening technique for high saliency interior permanent magnet motor," in *Proc. 38th IAS Annu. Meeting Conf. Rec. Ind. Appl. Conf.*, Oct. 2003, vol. 2, no. 2, pp. 898–905, doi: 10.1109/IAS.2003.1257641.

SOONHO KWON received the B.S. degree in electrical engineering from Myongji University, Gyeonggi-do, South Korea, in 2017, and the master's degree in automotive engineering from Kookmin University, Seoul, South Korea, in 2019, where he is currently pursuing the Ph.D. degree in automotive engineering. His research interests include the power converter/inverter design and permanent magnet ac motor control.

DONGKYUN SON received the bachelor's degree in electrical engineering from Ulsan University, Ulsan, South Korea, in 2017. He is currently pursuing the Ph. D. degree in automotive engineering with Kookmin University. His research interests include the electrical machine design/drive and control methods of multiphase electrical machines.

HEESUN LIM received the B.S. degree in mechanical and automotive engineering from Kookmin University, Seoul, Republic of Korea, in 2015, where she is currently pursuing the integrated master's and Ph.D. degrees with the Graduate School of Automotive Engineering. Her current research interests include the advanced control of electric machines and automotive inverters.

JIHWAN PARK received the M.S. degree in automotive engineering from Kookmin University, Seoul, South Korea, in 2019, where he is pursuing the Ph.D. degree in automotive engineering. His current research interests include the advanced control of electric machines and automotive inverters.

HYUNJUN BAEK received the B.S. degree in electronics engineering from Kookmin University, Seoul, South Korea, in 2016, where he is currently pursuing the Ph.D. degree in automotive engineering. His research interests include the inverter design and permanent magnet ac motor control.

GEUN-HO LEE received the B.S. and M.S. degrees in electrical engineering and the Ph.D. degree in automotive engineering from Hanyang University, Seoul, South Korea, in 1992, 1994 and 2010, respectively. From 1994 to 2002, he joined LG Industrial Research Institute, where he developed inverter system for elevators. Since 2011, he has been a Professor of automotive engineering with Kookmin University. His current research interests include the advanced control of electric machines and electric vehicles.